Common Precursor Mechanism for the Heterogeneous Reaction of D_2O, HCl, HBr, and HOBr with Water Ice in the Range 170−230 K: Mass Accommodation Coefficients on Ice

Benoît Fluckiger[†] and Michel J. Rossi*

Laboratoire de Pollution Atmosphérique et Sol (LPAS), Institut des Sciences et Technologies de l'Environnement (ISTE), Ecole Polytechnique Fédérale de Lausanne (EPFL), CH-1015 Lausanne, Switzerland

Received: August 27, 2002; In Final Form: February 26, 2003

A chemical kinetic model is presented which fits the uptake kinetics of both steady-state and time-resolved heterogeneous reactions of D_2O, HCl, HBr, and HOBr with ice substrates that have been studied in a Knudsen flow reactor. The salient feature of the model is the existence of two precursors to adsorption that explain the observed negative temperature dependence, as well as the absence of saturation, of the rate of uptake at the experimental conditions met in the Knudsen flow-reactor studies. From the temperature dependence of the fitted rate constants, enthalpy diagrams have been obtained in which the loosely bound precursor state has a binding energy on ice of 7.6−8.0, 6.4, 3.9, and 6.9 kcal/mol for D_2O, HCl, HBr, and HOBr, respectively. The mass accommodation coefficients α at 200 K were 0.43 (D_2O, B = bulk ice), 0.34 (D_2O, C = condensed ice), 0.67 (HOBr, B-type ice), 0.36 (HCl, B-type ice), and 0.38 (HBr, B-type ice) and show a negative temperature dependence as well. The chemical kinetic model describes the transition between submonolayer Langmuir adsorption at low to multilayer adsorption at high doses or partial pressures.

Introduction

Atmospheric ice has garnered much attention since it has been demonstrated that ice clouds in the stratosphere are to a significant degree involved in stratospheric ozone depletion.[1−5] Lately, cirrus clouds, as well as aviation contrails, occurring in the upper troposphere have been recognized as playing a crucial role in the radiative forcing of the atmosphere in relation to climate change.[6−8] It is increasingly being recognized that the chemistry−climate coupling is crucially important for climate prediction in addition to changes in atmospheric transport phenomena.[9,10] Therefore, the chemistry of atmospheric species occurring on atmospheric ice particles has received increased attention as of late.[11] Heterogeneous chemical processes occurring on polar stratospheric clouds (PSCs) during the polar night are not constrained by the kinetics because heterogeneous processing may take place essentially during the whole polar winter depending on the temperature so that interfacial reactions that have a low reaction probability will be equally important as compared to faster reaction probabilities. The situation is quite different with atmospheric chemistry occurring on cirrus clouds in view of their limited lifetime in the range from 30 min to several hours.[8,12] In this instance, the heterogeneous reaction kinetics plays a crucial role because it determines the time scale of chemical change occurring on atmospheric ice particles before they evaporate, if the laboratory results obtained on thin ice films have been obtained under conditions where they may be transferred to the properties of ice particles under atmospheric conditions.

There have been a number of fundamental experimental investigations on ice-catalyzed heterogeneous reactions occurring on mimics of PSCs or of upper tropospheric cirrus clouds with the emphasis placed on the measurement of the rate of uptake of the four title species. Questions remain concerning the exact nature of the interaction of the reactants with the ice cloud particles generated in the laboratory. When considering the overall complex kinetics of heterogeneous atmospheric reactions the interplay of processes, such as adsorption, desorption, and diffusion, in/on the condensed phase needs to be properly understood. These processes may be expected to vary considerably in their relative importance as type of ice, composition, and temperature changes occur. It is probably a cautious statement if we ascertain that for the foreseeable future realistic atmospheric conditions will not be obtained in laboratory experiments intended to explore the kinetics of atmospherically relevant multiphase reactive systems. Therefore, we need to extrapolate the kinetics of these reactions from the laboratory to the atmospherically relevant conditions. This is only possible if the reaction mechanism of the interfacial reaction system is known. In this respect it may be especially important to separate the uptake kinetics into elementary adsorption and desorption processes in order to obtain a complete understanding of the mechanism governing the behavior of the multiphase system. This separation may best be achieved by applying real-time or relaxation rather than steady-state rate techniques, the latter being routinely used for kinetic studies.

In this paper, we present a common chemical-kinetic precursor mechanism (Scheme 2, reaction sequence I+II) in terms of elementary gas and surface processes that is an extension of the one presented before,[16] which is able to account for experimental results of kinetic uptake measurements for M = $D_2{}^{18}O$ (H_2O),[13−16] HCl,[13,17−21] HBr,[20,22−24] and HOBr[25−28] interacting with ice in the temperature range 170−230 K.

The results of these studies encompassing steady-state uptake and real-time pulsed-dosing experiments in the presence of ice were recently obtained in our laboratory using a very low-pressure flow reactor operating in the molecular flow regime. Their uptake rates are all characterized by a strong negative temperature dependence implying the presence of a precursor

* Corresponding author. E-mail: michel.rossi@epfl.ch.
[†] Present address: Ecole Moser de Genève, 81, ch. De-La-Montagne, CH-1224 Chêne Bougeries (GE), Switzerland.

10.1021/jp021956u CCC: $25.00
Published on Web 04/30/2003

SCHEME 1

$$M_{(gas)} \underset{F_{ev}}{\overset{k_{ads}}{\rightleftharpoons}} M_{(bulk)}$$

SCHEME 2

$$M + S \leftrightarrow P_1 \qquad k_1, k_{-1}$$
$$P_1 \leftrightarrow B + S \qquad k_2, k_{-2} \qquad \text{Sequence I}$$

$$M + P_1 \leftrightarrow P_2 \qquad k_3, k_{-3}$$
$$P_2 \leftrightarrow B + P_1 \qquad k_4, k_{-4} \qquad \text{Sequence II}$$

to adsorption which leads to a complex mechanism. We have established the reaction enthalpy from the activation energies of the fitted rate constants for the four reactions of M which clearly show the existence of two stable precursor states of M in the condensed phase in addition to the thermodynamically stable condensed phase of M.

Experimental Details

The experiments were performed in a Teflon coated Knudsen flow reactor operating in the molecular flow regime. This technique has been described in great detail in the literature.[29,30] Briefly, the gases under study were introduced into the Knudsen reactor from the gas handling line by using a flow-controlling device, either a glass capillary or a pulsed solenoid valve. The gases leave the Knudsen reactor through an escape orifice whose variable diameter (1−14 mm) determines the residence time and the concentration inside the flow reactor over a range of a factor of 200. The characteristic parameters of the reactor are given in Table 1. The modulated effusive beam leaving the Knudsen cell is analyzed by a quadrupole mass spectrometer (MS) whose settings were chosen to yield a sensitivity of approximately 10^{10} molecule cm^{-3} at a signal-to-noise ratio greater than 2. An isolation plunger allows the separation of the reactive substrate located in the sample chamber from the reactor volume. *Pulsed-valve experiments* were performed by introducing a known dose in the range $10^{14}-10^{16}$ molecules into the reactor across a solenoid valve at a pulse duration of a few milliseconds. The observed single-exponential decay in the presence of a reactive surface is characterized by a rate constant k_{eff} which is the sum of the escape rate constant k_{esc} and the pseudo-first-order reaction rate constant equal to k_{uni} (Table 1). The rate constant for effusive loss k_{esc} is determined by fitting an exponential decay function to the experimental MS signal trace in the absence of reaction. The second type of experiment was a continuous-flow or *steady-state experiment* which was performed by introducing a constant flow of molecules through a capillary into the flow reactor. The change of the MS signal level of the corresponding compound upon opening (S°) and closing (S^i) the sample chamber resulted in a value for the net uptake coefficient γ on a per collision basis (Table 1). A low-temperature sample support in which the sample could be cooled to 150 K was used. A programmable temperature controller maintained the final temperature to ±0.5 K at an accuracy of ±2 K.

Preparation of the Ice Samples. For the preparation of bulk (B) ice samples, approximately 5 mL of degassed distilled water (H_2O) were poured into the sample support at ambient temperature and cooled to the desired temperature in about 15 min and subsequently evacuated. To avoid the inclusion of air bubbles in the crystal, the water had previously been degassed by freeze−pump−thaw cycles on a vacuum line. For condensed (C) ice, the mounted and evacuated sample support was cooled to the desired temperature, usually in the range 160−180 K, followed by condensation of H_2O vapor from the gas phase at a typical flow rate of $F = 10^{18}$ molecule/s. The calculated thickness using the known density of ice of 0.92 g cm^{-3} for low-temperature (C) samples was in the range 2−10 μm. All experiments used in this work have been performed on "desorbing" ice samples, that is, without adding an external flow of H_2O vapor that usually compensates for the rate of H_2O evaporation from the ice sample. For the studies concerning $D_2{}^{18}O$ on ice, the ice samples have been prepared from $D_2{}^{16}O$ vapor in order to separate the evaporation rate of unlabeled D_2O desorbing from the ice matrix from the condensation and evaporation[31] rate of the labeled probe molecules.

TABLE 1: Characteristic Parameters and Relevant Kinetic Expressions of the Reactor Used for the Experimental Results

definition	value
reactor volume V	$V = 2000$ cm^3
estimated internal reactor surface area A_R	$A_R = 1300$ cm^2
sample geometric surface area A_S	$A_S = 15$ cm^2
gas number density $N = F/(Vk_{esc})$	$1-1000 \times 10^{10}$ cm^{-3}
F = flow into the reactor [molecule s^{-1}]	
escape rate constant for o.d. 14 mm aperture (exptl) at 300 K	$k_{esc}(D_2{}^{18}O) = 6.6 \pm 0.3$ s^{-1} $k_{esc}(HCl) = 5.6 \pm 0.2$ s^{-1} $k_{esc}(HBr) = 3.0 \pm 0.1$ s^{-1} $k_{esc}(HOBr) = 3.1 \pm 0.1$ s^{-1}
first-order rate constant k_{uni} [s^{-1}]	$k_{uni} = (S^i/S^o - 1)k_{esc}$ with S^i, S^o being the initial and steady-state MS signals, respectively
collision frequency ω [s^{-1}]	$\omega = \langle c \rangle / 4VA_S = 0.863\sqrt{T/M}$ $\langle c \rangle$ = mean molecular speed in m/s T = room temperature = 300 K M = molecular mass in kg/mol
uptake coefficient γ	$\gamma = k_{uni}/\omega$
MS detection	$D_2{}^{18}O$: $m/e = 22$ $D_2{}^{16}O$: $m/e = 20$ HCl: $m/e = 36$ HBr: $m/e = 80$ HOBr: $m/e = 97$

Brief Survey of Experimental Results. We have chosen four prototypical heterogeneous reactions of importance to atmospheric chemistry involving the species M = $D_2{}^{18}O$, HCl, HBr, and HOBr interacting with H_2O ice because the kinetic results have all been obtained using the same experimental method which facilitates cross comparison.

(A) The Negative Temperature Dependence of the Rate of Uptake. A negative activation energy E_a for the rate of uptake of $D_2{}^{18}O$ on ice has been found by Chaix et al.[16] who observed two distinct regimes of temperature dependence of the uptake coefficient γ. The values at low temperatures (140−200 K) lead to a negative activation energy of $E_a = -0.25 \pm 0.08$ kcal/mol, whereas at high temperatures (200−230 K), γ changes more rapidly with temperature compared to the low-temperature regime, in agreement with an activation energy of $E_a = -4.3 \pm 1.5$ kcal/mol. The higher value of E_a was attributed to competitive evaporation resulting in a significant decrease of the net $D_2{}^{18}O$ uptake. No dependence of E_a on the type of substrate has been found. On the other hand, the absolute value of the uptake coefficient γ depends on the type of ice substrate, sample preparation, and sample thermal history such as annealing episodes.

For the experiments concerning the interaction of HOBr on ice,[28] the values of the initial uptake coefficient γ_o on different types of pure H_2O ice, namely, single-crystal (SC), vapor-deposited (C), and samples frozen from liquid H_2O (B) ice, range from 0.4 to 0.03 in the range 175−205 K, thus revealing a pronounced negative temperature dependence corresponding to an activation energy of $E_a = -9.7 \pm 1.0$ kcal/mol. However, at any given temperature the rate of HOBr uptake is independent of the type of ice. It has to be noted that such a strong temperature dependence of the HOBr rate of uptake on ice has also been observed in flow-tube experiments.[25,27]

A considerable number of experimental and modeling studies exists concerning the interaction of HCl with water-ice at atmospherically relevant temperatures owing to the atmospheric importance of the fast heterogeneous reaction of $ClONO_2$ (chlorine nitrate) with HCl adsorbed on ice (HCl_{ads}). Most of this research agrees with the fact that HCl exists in/on the ice substrate in ionic form $H_3O^+\cdots Cl^-$ following adsorption. In the temperature range 190−210 K, a negative temperature dependence of the rate of uptake of HCl has been observed with γ ranging from 0.34 to 0.22 at 190 and 210 K, respectively, at low HCl partial pressure of 10^{-6}−10^{-4} Torr, which is in agreement with a negative activation energy of $E_a = -1.8 \pm 0.5$ kcal/mol. The interaction of small HCl concentrations with ice leads to an HCl/ice mixture called "quasi-liquid", whereas at higher HCl partial pressure of 10^{-4}−10^{-3} Torr the interaction of HCl with ice results in the formation of a liquidlike layer atop the ice substrate. This liquidlike mixture is characterized by the equilibrium vapor pressure indicated by the solid−liquid coexistence line in the HCl/ice-phase diagram.[50] It means that any further increase of the quantity of HCl to the system will not have an effect on the HCl partial pressure as the saturation (vapor) pressure has already been attained. Instead, any additional quantity of HCl will be dissolved in the condensed phase, thereby dissolving more crystalline ice in order to keep the HCl concentration in the condensed phase constant. Instead, the quasi-liquid state of HCl/ice leads to a HCl partial pressure that is lower than the limiting vapor pressure given by the coexistence line. Any addition of HCl to the system in the quasi-liquid state will lead to an increase in HCl partial pressure whose exact value will depend on structural parameters of the ice matrix. In this latter case, a more pronounced negative activation energy for HCl adsorption of $E_a = -3.1 \pm 0.5$ kcal/mol has been found.

The temperature dependence of the rate of HBr adsorption on ice follows the general trend observed for the above three examples. A negative activation energy of $E_a = -1.7 \pm 0.5$ kcal/mol was observed in the temperature range 190−210 K. This value increased to $E_a = -3.9 \pm 0.5$ kcal/mol at higher temperature (210−225 K).[20,49] At 225 K, the upper limit of our measurement range, γ(HBr) was found to be equal to 0.12. It has to be noted that this value is significantly larger than the one measured by another group who found a value of γ(HBr) = 0.03 using the coated-wall flow-tube technique[24] and who concluded that γ was essentially independent of temperature in the range 212−228 K. This disagreement of a factor of 4 is not yet understood, although many reasons may be invoked, such as the protocol for ice preparation, the effect of the diffusion limit on the uptake kinetics in the case of the flow-tube experiments, or underestimation of the total reactive surface area in the Knudsen cell experiments.

(B) Partial Saturation of the Reactive Substrate and Establishment of the Equilibrium Vapor Pressure. With the exception of HBr, the establishment of a partial pressure of M over ice has been observed in both steady-state and pulsed-valve experiments for M = HCl/ice[20] and HOBr/ice[28] once a sufficient quantity of M had been adsorbed. For HCl, the results have been interpreted in terms of a mechanism involving the adsorption and the subsequent ionization of HCl at the interface, HCl desorption, and a slow but measurable loss of HCl by diffusion from the interface into the bulk,[32] which was characterized as a Fickian diffusion coefficient D_{HCl}. This scheme is almost certainly also valid for the case of HOBr, for which the experimental observables are very similar to HCl. During continuous-flow experiments of HCl uptake on ice, a partial saturation of the rate, that is, a decrease of γ_0 leading to a higher steady-state partial pressure, was systematically observed.[20] At this partial saturation, the ice substrate was able to support a measurable vapor pressure of HOBr and HCl, once the HOBr or HCl source was shut off. A van't Hoff plot of the equilibrium vapor pressures leads to $\Delta H^0_r = -9.4 \pm 1.0$ kcal/mol for HOBr[28] and -8.5 ± 1.0 kcal/mol for HCl.[20] In addition, pulsed-dosing experiments also support a vapor pressure at sufficiently high dose once the transient supersaturation has subsided. The pulsed-valve experiments of $D_2{}^{18}O$ interacting on a $D_2{}^{16}O$ ice substrate were conducted on various types of ices[16] and revealed the same behavior at high dose as observed for the pulsed uptake experiments of HOBr-ice and HCl-ice, namely, the occurrence of a constant flow rate F_{SS} owing to evaporation in the aftermath of the pulse for as long as the supply of adsorbed labeled D_2O molecules lasts (Figure 1b). The absolute value of F_{SS} was found to depend only on the temperature of the ice substrate and therefore led to an equilibrium between the rate of condensation $R_{ads} = k_{eff}[D_2{}^{18}O]$ with $k_{eff} = k_{ads}$ and evaporation R_{ev} of $[D_2{}^{18}O]_{ads}$ from the surface. In contrast to the above three reactions, no rate of desorption could be measured in the case of the interaction of HBr with an ice substrate.

(C) Apparent First-Order Rate Constant for Adsorption. The experimentally determined rate law for adsorption of M is first order in [M], the gas-phase concentration of M, and $\gamma_0 = k_{eff}/\omega$ was found to be independent of [M] at low concentration. We emphasize that both pulsed-valve and steady-state experiments are complementary as far as the time evolution of the gas-phase concentration in the reactor is concerned: for pulsed-valve experiments the coverage of the reactive surface is very slight at low dose, on the order of 5% of the total reactive surface or less. Therefore, the rate of uptake given by k_{eff} determined under these conditions is only controlled by adsorption without any significant contribution of desorption to the MS signal owing to the small surface coverage. The value of γ_0 in this case approaches the mass accommodation coefficient α. At increasing dose, the rate of uptake is slowing down because of partial saturation of the substrate surface and leads to desorption of initially adsorbed molecules, thus complicating the experimental separation into the rates of adsorption and desorption. The effect of desorption is clearly visible in steady-state experiments in which the net uptake decreases from the high value of γ_0 to a lower value γ_{ss} on a time scale depending on the flow rate of M into the reactor. This partial saturation process may be modeled by the initial adsorption of molecules on reactive surface sites following a Langmuir adsorption model that leads to a steady-state rate of adsorption and desorption. At high [M], the equilibrium between adsorption and desorption is rapidly established such that γ_{ss} represents the net uptake consisting of adsorption to and desorption from the ice substrate.

We will briefly describe below how the relevant kinetic parameters, such as uptake coefficient, rate of desorption, and equilibrium vapor pressure, may be obtained from experimental

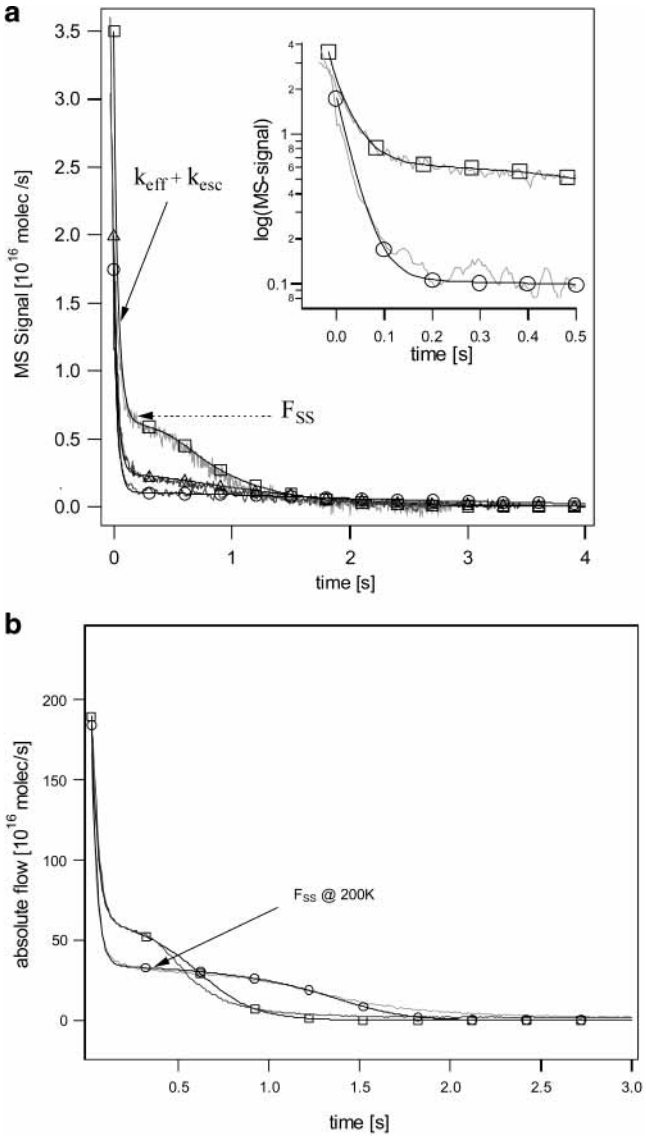

Figure 1. (a) Comparison between experimental (gray trace) and simulated (smooth lines) pulsed-valve experiments of HCl on bulk ice at (○) 190, (△) 200 K, and (□) 210 K. Raw data were taken from ref 20. The input doses are 3.5×10^{15}, 4×10^{15}, and 7×10^{15} molecules per pulse at 190, 200, and 210 K. The value of k_{eff} is assessed according to an exponential fit of the first part of the decay curves of the reactive traces. The value of F_{SS} is determined as shown in the figure. The inset displays the MS signal on a semilogarithmic scale, revealing the first-order rate of decay of the reactive pulse. (b) Comparison between experimental and simulated pulsed-valve experiments of $D_2{}^{18}O$ on $D_2{}^{16}O$ ice at (○) 200 and (□) 205 K. The injected dose is 4.5×10^{17} molecules per pulse for both cases. Such temperature-dependent MS traces are used for the determination of the constants k_2 and k_{-2} in the model in that they control the shape of the decay of the quasi steady-state MS signal F_{SS} in the aftermath of the pulse.

data in order to provide a solid basis of comparison for the modeling effort.

Review of the Kinetic Formalism. For doses exceeding a certain threshold value, the formation of a steady-state level is observed after the pulse decay in pulsed-valve experiments. Figure 1a represents such experiments of HCl on ice at three temperatures. The injected doses were 4×10^{15} at 190 K, corresponding to 44% of a molecular HCl monolayer if all the molecules were adsorbed; 5×10^{15} at 200 K; and 8×10^{15} molecules per pulse at 210 K. The value of k_{eff} is determined from a single-exponential fit to the experimental trace in the range 0−100 ms as shown in the inset of Figure 1a. At 200 ms, the MS signals tend to a steady-state value F_{SS} whose duration was found to depend on the value of the injected dose and whose absolute value only depends on the temperature of the ice substrate. This level results from the equilibrium vapor pressure of HCl at steady-state sustained by the rate of evaporation R_{ev}, which persists for a given time depending on the quantity of HCl deposited on top of bulk H_2O ice. Note that the value k_{eff} is a *net* rate constant resulting from both adsorption and desorption rates. The value of the rate constant for adsorption k_{ads} may be determined in experiments performed at low dose in order to minimize the desorption of molecules adsorbed within a given pulse. This is the case for the low doses in the submonolayer regime applied in this work that typically leads to the adsorption of 90% of the applied dose within the first 100 ms after the admission of the pulse ($\gamma_0 = 0.3$ at 190 K; ω (300 K, HCl) = 78.4 s^{-1}). Under these conditions the measured uptake coefficient γ_0 approaches the mass accommodation coefficient α as will be discussed below. The rate of evaporation F_{ev} in units of molecule/s is determined from the observed steady-state level F_{ss} that appears after the pulse and is calculated following eq 1 on the basis of a simple two-state equilibrium model for HCl condensation and evaporation where k_{ads} is equal to k_{eff} and is determined in pulsed experiments at low HCl dose. This simple two-state reaction system (Scheme 1) summarizes the thermochemistry of the two-phase system and preserves its validity despite the incidence of a complex reaction mechanism to be discussed below. In summary, we have used pulsed-injection experiments performed in real time and at low doses which describe the approach to steady state in order to enable the separation of the uptake rate into the rate of adsorption ($k_{ads} = k_{eff}$) and desorption (F_{ev}).

$$F_{ev} = F_{ss}\left(1 + \frac{k_{ads}}{k_{esc}}\right) \tag{1}$$

With kinetic data on adsorption or condensation, k_{ads}, and desorption or evaporation, F_{ev},[31] the equilibrium vapor pressure P_{eq} of HCl in units of Torr may be calculated according to eq 2:

$$P_{eq} = \frac{F_{ev}}{k_{ads}V}RT \tag{2}$$

Similar kinetic observations were made for the reactive systems HOBr/ice and $D_2{}^{18}O$ on $D_2{}^{16}O$ ice (Figure 1b) whose kinetic parameters were therefore assessed in the same way.

Steady-state experiments may serve as complementary experiments that are especially useful for low partial pressures of M. Figure 2 displays a typical experiment of HCl on B-type ice at 190 K at a flow rate $F_i = 7.6 \times 10^{14}$ molecule/s where the surface is first exposed to HCl at $t = 105$ s. We observe an initial high rate of uptake of HCl leading to a small MS signal F_0 ("spike") at the beginning of the interaction, followed by a second higher steady-state level F_{ss} at $t = 110$ s, which corresponds to a lower net uptake rate characterized by γ_{ss}. According to Scheme 1, the rate of desorption F_{ev} may be calculated for steady-state experiments according to eq 3 using k_{ads} determined from pulsed-valve experiments:

$$F_{ev} = F_{ss}\left(1 + \frac{k_{ads}}{k_{esc}}\right) - F_i \tag{3}$$

The equilibrium vapor pressure of HCl is then calculated according to eq 2. We emphasize that the large first-order rate constant for uptake $k_{uni} = (F_i/F_0 - 1)k_{esc}$ (Table 1) obtained at

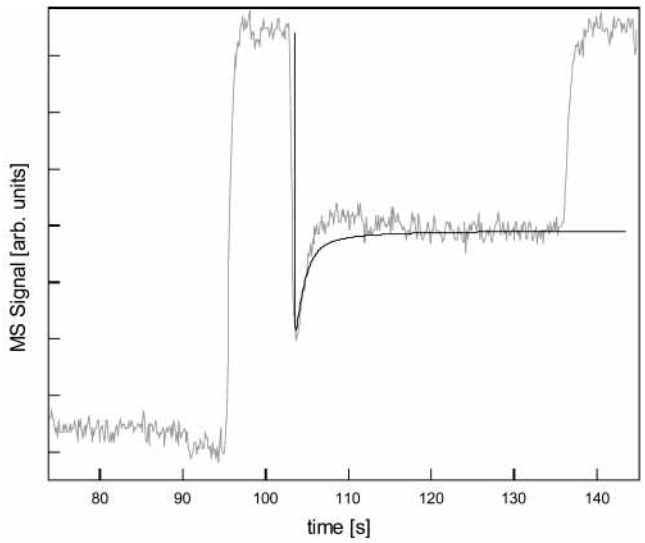

Figure 2. Steady-state experiment of HCl interacting with bulk (B) water ice performed at 190 K using the 8 mm orifice. Raw data were taken from ref 49. The initial flow of HCl is $F_i = 7.6 \times 10^{14}$ molecule/s. The solid line is the result of the model at this flow rate using the constants displayed in Table 2.

the beginning of steady-state uptake experiments leads to the same numerical value as k_{eff} at low HCl doses in pulsed-valve experiments. Thus we have $k_{uni} = k_{eff}$ for low flow rates and low doses of M in steady-state and pulsed-valve experiments, respectively.[20] As indicated before, γ_0 approaches the value of α under these special conditions, even for steady-state experiments.

The steady-state rate of uptake is controlled by partial saturation of the free adsorption sites on the substrate in terms of a Langmuir model of molecular adsorption. This points to a complex uptake mechanism under steady-state conditions including desorption of $M_{(ads)}$ with M = HCl, HOBr, and $D_2{}^{18}O$. This counteracts the adsorption of M on the ice substrate resulting in a *net* rate of uptake described in terms of the uptake coefficient γ_{ss}. The occurrence of a transient, sometimes pseudo-steady-state level F_{ss}, observable in Figure 1a,b in pulsed-valve experiments, corresponds to the equilibrium between the rate of adsorption and desorption which is perturbed to a variable extent by the escape rate of effusion out of the flow reactor. The rate of desorption is independent of the injected dose which however controls the duration of the steady-state level. A single pulsed-valve experiment enables the separation of the net rate of uptake of M into the elementary rates of adsorption and desorption according to Scheme 1 provided the quantity of deposited molecules was large enough to support a quasi-steady-state rate of evaporation of M in the aftermath of the pulse as displayed in Figure 1a,b. This separation of the net rate of uptake may in principle also be achieved using two independent data sets obtained in steady-state experiments. This method, however, is hampered in practice by the difficulty of obtaining two significantly different data sets.

The chemical kinetic model to be presented below will therefore have to fit the following main results obtained from the kinetic investigations summarized above:

•the apparent rate law first order in M observed under all relevant experimental conditions;

•the negative temperature dependence of k_{eff}, k_{uni}, or γ_0 resulting from the pulsed-valve experiments which calls for the existence of a precursor to molecular adsorption as has been suggested before;[16,27,33]

•the partial saturation of the uptake as observed in steady-state experiments at low pressures (flow rates) which leads to a time-dependent rate of uptake;[20]

•the inability to fully saturate the uptake at high doses in pulsed-valve and at high partial pressures in steady-state experiments;

•the constant or near-constant rate of evaporation at high doses/partial pressures as well as at low doses/partial pressures, respectively, which only depends on temperature. The former situation corresponds to the vapor pressure of the liquid−solid coexistence line in the HCl/ice-phase diagram[34] and the latter to a thermodynamic state of the quasi-liquid HCl/ice adsorbate below the coexistence line. The obvious exception is the HBr/ice system, for which no rate of evaporation could be measured up to 220 K, because it presumably is below our detection limit.

The Chemical-Kinetic Model. The goal of this work was to find a set of kinetic constants that gives the best fit to the measured time-dependent MS signal S(t) which is related to the instantaneous gas-phase concentration in the reactor according to $[M(t)] = \beta I(t)/k_{esc}V$. The factor β is derived from ancillary calibrations of the MS signal $I(t)$ of M with absolute flow rates obtained by measuring the pressure change in a calibrated volume as a function of time. Both pulsed and steady-state experiments over a range of temperatures, flow rates, and orifice diameters were used to obtain the fitting parameters. Special emphasis was placed on the dependence of the uptake coefficient on the temperature as well as on the values of the rate of adsorption and desorption of M as a function of its initial partial pressure over ice. To fit the experimental data, we propose the precursor mechanism displayed in Scheme 2, which consists of the reaction sequence I+II and which we briefly presented in the Introduction.

In reaction sequence I, a gas-phase species M is trapped by a reactive surface site S on the ice substrate in an accommodation process k_1 characterized by an accommodation coefficient $\alpha = k_1/\omega$. This adsorption, characterized by the adsorption rate constant k_1, results in the formation of the precursor species P_1 which consists of adsorbed M (M_{ads}) located at the interface region of the substrate surface. Subsequently, the precursor species may desorb into the gas phase in a first-order process k_{-1} or it may rearrange to a thermodynamically stable species $B = M_{bulk}$ in a first-order process k_2. According to sequence I, the decay rate constant $k_{dec} = k_{esc} + k_{eff}$ in a reactive pulsed-valve experiment scales with both the time-dependent available number of reactive sites $\{S(t)\}$ and the surface concentration $\{P_1(t)\}$ of the precursor species according to eq 4:

$$k_{dec} = k_{esc} + k_1\{S(t)\} - k_{-1}\left(\frac{\{P_1\}}{[M]_{(g)}}\right)(t) \qquad (4)$$

From eq 4 it is obvious that the decay rate constant k_{dec} would tend toward the limiting value k_{esc} at large dose which corresponds to the replacement of the surface sites $\{S(t)\}$ with the precursor species P_1 leading to the saturation of the surface for further adsorption of M. A competitive pathway for adsorption of M (sequence II) had to be added to reaction sequence I in order to account for the fact that no saturation of the rate of uptake of M has experimentally ever been observed, even at large doses of M.

Scheme 2 consists of reaction sequence I+II. Sequences I and II are competitive pathways ultimately transforming a molecule M on accommodation into a stable condensed-phase species $B = M_{bulk}$ within the ice. The physical nature of M_{bulk} or B may be, for instance, $H_3O^+\cdots Cl^-$ for HCl, $H^+\cdots BrO^-$,

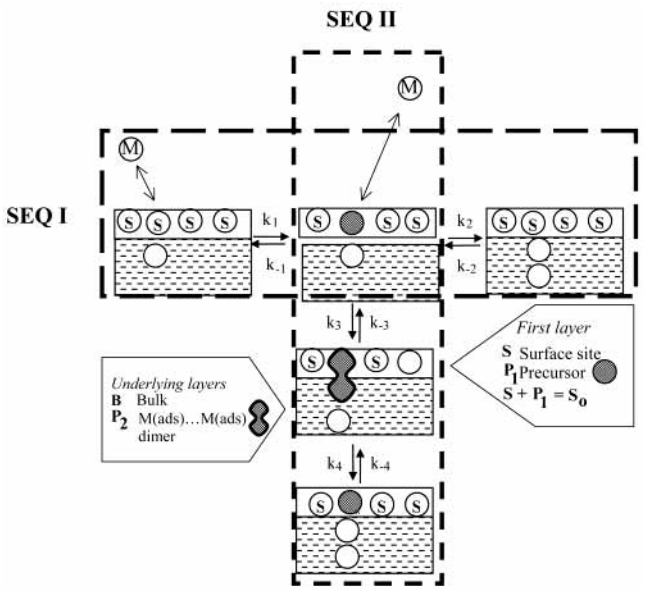

Figure 3. Schematic illustration of the competitive processes occurring on the surface according to Scheme 2. Sequence I is displayed horizontally starting with adsorption of M on free reaction sites S, whereas sequence II corresponds to the vertical reaction sequence and is initiated by adsorption of M on the $P_1(M_{ads})$ precursor species. P_2 is the dimer $M_{ads}\cdots M_{ads}$; $B(M_{bulk})$ is the stable condensed-phase state of M.

$HOBr\cdot nH_2O$, or $H_3O^+BrO^-\cdot nH_2O$ for HOBr. We would like to stress, however, that we are unable to associate the chemical changes described in Scheme 2 to either its molecular identity or to its corresponding physical location in terms of the structure of the ice/atmosphere interface of the substrate because the scope of the present work is entirely kinetic.

The branching between sequences I and II strongly depends on the injected dose. In fact, sequence I saturates the surface sites transforming S_0 sites into P_1. Sequence II controls the kinetics of condensation and evaporation for $M = D_2O$ or of adsorption and desorption for M = HCl, HBr, and HOBr at high dose or high steady-state flow rate when the precursor species P_1 has replaced the free surface sites $S = S_0 - P_1$ and are thus acting as surface sites for further adsorption of M in sequence II. It fulfills a very important purpose at high doses or partial pressures, namely, that it prevents the saturation of adsorption of M on the substrate in that it regenerates the active sites P_1 for adsorption in process k_4.

We assume that the elementary adsorption step k_1 of M follows the Langmuir ansatz for adsorption and thus obeys a first order rate law in both M and {S} at early reaction times and low concentrations where the reverse process, first-order desorption, may be neglected. The overall rate process, however, is effectively a second-order process that is the hallmark of the Langmuir ansatz of surface kinetics. A sketch of the different processes occurring at the surface of the ice is shown in Figure 3.

According to Scheme 2, the time evolution of the partitioning between the gas-phase concentration [M] (square brackets, []) and the surface density (curved brackets, {}) of the various condensed-phase species of M, namely, $\{P_1(t)\}$, $\{P_2(t)\}$, $\{S(t)\}$ (free surface sites), and $\{B(t)\} = \{M_{bulk}\}$, respectively, may be given by solving a set of coupled rate equations given in eqs E-1−E-4 under the constraint of $\{S(t) + P_1(t)\} = S_0$, the number of reactive surface sites at $t = 0$. In these equations, the brackets denoting concentrations in the gas phase and at the interface or in the bulk have been omitted for convenience:

$$d\{M(t)\}/dt = -k_{esc}\{M(t)\} - k_1\{M(t)\}(S_0 - \{P_1(t)\}) + k_{-1}\{P_1(t)\} - k_3\{M(t)\}\{P_1(t)\} + k_{-3}\{P_2(t)\} \quad \text{(E-1)}$$

$$d\{P_1(t)\}/dt = k_1\{M(t)\}(S_0 - \{P_1(t)\}) - (k_{-1} + k_2)\{P_1(t)\} + k_{-2}\{B(t)\}(S_0 - \{P_1(t)\}) - k_3\{M(t)\}\{P_1(t)\} + (k_{-3} + k_4)\{P_2(t)\} - k_{-4}\{B(t)\}\{P_1(t)\} \quad \text{(E-2)}$$

$$d\{P_2(t)\}/dt = k_3\{M(t)\}\{P_1(t)\} - (k_{-3} + k_4)\{P_2(t)\} + k_{-4}\{B(t)\}\{P_2(t)\} \quad \text{(E-3)}$$

$$d\{B(t)\}/dt = k_2\{P_1(t)\} - k_{-2}\{B(t)\}(S_0 - \{P_1(t)\}) + k_4\{P_2(t)\} - k_{-4}\{B(t)\}\{P_2(t)\} \quad \text{(E-4)}$$

The kinetic parameters corresponding to the set of the eight rate coefficients used in this work and the adjustable parameter S_0 are displayed in Table 2. Specifically, the reaction probability of M hitting a free surface site S was set equal to the one for P_1, which leads to the dimer species P_2 in process k_3 of Scheme 2. This may also be seen by inspection of Table 2. To be able to obtain good fits for the temperature dependence of the uptake rate performed at low doses, typically less than 10^{15} molecules per pulse for HCl for example, it has been necessary to introduce a weak temperature dependence for S_0 ranging from 2.5×10^{15} at 190 K, 2.0×10^{15} at 200 K to 1.0×10^{15} at 215 K corresponding to 1.7×10^{14}, 1.3×10^{14}, and 6.7×10^{13} molecule cm^{-2}, respectively. This set of S_0 has been used for all four members of the series. Such a negative temperature dependence corresponds to an activation energy of $E_a = -2.2 \pm 0.1$ kcal/mol. The surface density of active sites for adsorption of M on ice resulting from the model is significantly smaller than the surface density of H_2O on ice of 9.9×10^{14} molecule cm^{-2} ($\rho = 0.93$ g cm^{-3}), the surface density of HCl (6.0×10^{14} molecule cm^{-2}, $\rho = 0.879$ g cm^{-3}), or the surface density of HBr (7.4×10^{14} molecule cm^{-2}, $\rho = 2.717$ g cm^{-3}) using published densities of the pure condensed phase.[35] This shows that only a fraction of the geometric surface area of the ice substrate has the ability to bind the precursor state of M that is the gateway to the condensed phase in the uptake of M on ice. We are able to state the magnitude of S_0 with confidence because it is related to the fact that we observe the onset of saturation of the adsorption of M at specific doses that have been accurately measured in reference experiments.

Two research groups have recently established the surface coverage at saturation for HCl on ice. Lee et al.[36] have measured a saturation coverage of $(1.1 \pm 0.6) \times 10^{14}$ molecules cm^{-2} at 201 K and Hynes et al.[21] $(2.0 \pm 0.7) \times 10^{14}$ molecules cm^{-2} at 205 K. Our value agrees within a factor of 2 with the mean which is satisfactory given the uncertainties of the individual measurements. This corroborates the above conclusions on the absolute magnitude of S_0. For HBr, unlimited uptake has been observed as the rate of uptake leading to HBr hydrates proceeds without kinetic limitations up to the point where spontaneous disintegration of the ice film accompanied by desorption of HBr occurs.[37] The quantity of HBr taken up on a 1.1 ± 0.2 μm thick ice film increases linearly with HBr partial pressure from 1.0×10^{14} molecule cm^{-2} at 10^{-7} Torr to 1.1×10^{15} molecule cm^{-2} at 10^{-6} Torr at 195 K. Experiments of HOBr uptake in a coated-wall flow tube resulted in the uptake of large amounts of HOBr on an ice film over typically 150 min, typically 2.9×10^{16} molecules cm^{-2} at 10^{-6} Torr of HOBr at 198 K.[27]

Equations E-1−E-4 ensure that the total number of the two reactive sites $S(t)$ and $P_1(t)$ never exceeds the initial number of geometric surface sites S_0 whose value has been discussed

TABLE 2: Kinetic Parameters for the Modeled Rate Constants for $D_2{}^{18}O/D_2{}^{16}O$ Ice, $HOBr/H_2O$ Ice, HCl/H_2O Ice, and HBr/H_2O Ice[a]

rate constant[b]	$D_2{}^{18}O$ log(A)[c]	B E_a[d]	$D_2{}^{18}O$ log(A)[c]	C E_a[d]	HOBr og(A)[c]	B E_a[d]	HCl log(A)[c]	B E_a[d]	HBr log(A)[c]	B E_a[d]
k_1 (molecule^{-1} s^{-1})	−13.75	0	−13.85	0	−13.88	0	−13.94	0	−14.09	0
k_{-1} (s^{-1})	11.30	7.6	11.62	8.0	8.20	6.9	7.93	6.4	1.97	3.9
k_2 (s^{-1})	4.73	4.0	2.84	4.0	1.32	0.4	6.14	5.0	6.03	3.0
k_{-2} (molecule^{-1} s^{-1})	−5.02	8.0	−7.17	8.0	−7.74	4.9	−5.62	7.0	−6.90	6.1
k_3 (molecule^{-1} s^{-1})	−13.5	0	−13.85	0	−13.88	0	−13.97	0	−14.09	0
k_{-3} (s^{-1})	16.33	11.6	16.31	11.6	17.30	11.6	12.31	9.0	9.02	6.6
k_4 (s^{-1})	4.17	0	4.17	0	4.00	0	3.90	0	3.47	0
k_{-4} (molecule^{-1} s^{-1})	−20.00	0	−20.00	0	−20.00	0	−20.00	0	−20.50	0
ΔH_{sub} (kcal/mol)		11.6		12		11.4		8.4		7.0

[a] B is bulk ice; C is condensed ice (see text). [b] The rate constants are expressed according to $k(T) = A \exp(-E_a/RT)$, with $R = 1.987$ cal mol^{-1} K^{-1}. [c] log(A) is expressed in molecule^{-1} s^{-1} for the second-order rate constants k_1, k_{-2}, k_3, and k_{-4}, and in s^{-1} for the first-order rate constants k_{-1}, k_2, k_{-3}, and k_4. [d] E_a is expressed in kcal/mol.

above. The P_2 precursor may be regarded as a dimer form of M or a complex between M and P_1 that is incorporated into the interface region of the ice matrix (see Figure 3). In contrast to P_1, whose maximum value is S_0, P_2 and B are allowed to grow indefinitely as a function of the partial pressure of M. The quantity of the second precursor P_2 depends on the dose of M and together with B acts as a reservoir for adsorbed M, namely, P_1. Owing to the microscopic reversibility of the interfacial reaction system, the gateway of the condensed phase of M to the gas phase leads through evaporation across both intermediates P_1 and P_2. Therefore, the direct pathway from B to M in Scheme 2 is thereby precluded.

The rate of desorption of M from the reservoir is sometimes controlled by the physical properties of the ice substrate at the gas-condensed-phase interface and is expressed in the model as $k_{-1}P_1(t)$. An example of this behavior may be found when comparing the kinetics of B- or C-type ice for $M = D_2{}^{18}O$ where moderate or high doses of M give rise to evaporation in the aftermath of water pulses for B-type but not for C-type ice as displayed in Figure 1b. In fact, it is the rate constants k_2 and k_{-2} that control the amount of $P_1(t)$ and therefore the elementary rate of evaporation $k_{-1}P_1(t)$ as will be discussed below. Table 2 shows that k_{-1} for $D_2{}^{18}O$ on B- and C-type ice is identical, whereas both k_2 and k_{-2} are markedly different for both types of ice because the preexponential factors of k_2 and k_{-2} for C-type ice are both smaller by 2 orders of magnitude compared to B-type ice. In addition to a slight shift of the equilibrium between P_1 and B in favor of the bulk-state B, for C-type ice the important effect seems to be the change of the time scale by 2 orders of magnitude. It is longer for the C-type compared to that for B-type ice in regards to the rearrangement of P_1 to B in process 2. On the other hand, such a dependence of the rate of evaporation on the type of ice has not been found in the temperature range of interest in experiments for M = HCl and HOBr. The reason for this difference is at present not understood, despite the fact that the present chemical-kinetic model properly simulates the reaction kinetics in all cases.

Figure 4 displays the time evolution of HCl (gas) and of the condensed-phase products HCl(P_1), HCl(P_2), and HCl(B) simulated for three different doses at 210 K. At a low dose of 10^{13} molecules, which corresponds to a surface coverage of 7.5%, no steady state is observable in the gas phase. The corresponding maximum value of P_1 is 4×10^{12} sites, which represents 0.3% of S_0. Therefore, the value of the first-order rate constant k_{eff} obtained by fitting the simulated trace M corresponding to the full circles on the upper part of Figure 4 leads to the value $k_1S_0 = 17$ s^{-1} and may be identified with k_{ads} at 210 K. At a dose of 7×10^{15} molecules, the steady-state level is observed for a

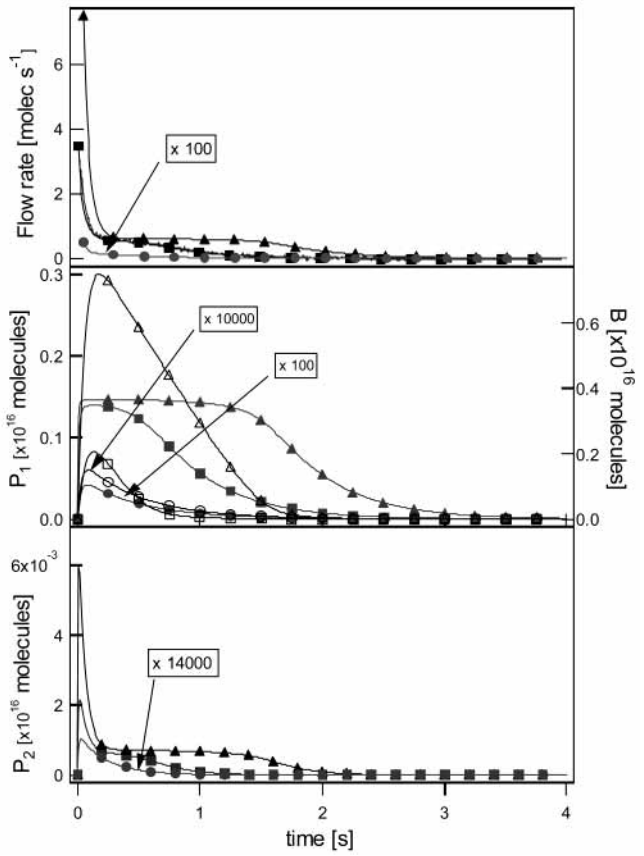

Figure 4. Time evolution of the gas-phase M(t) (top) and the condensed-phase products $P_1(t)$ and B(t) (middle) in the case of the interaction of HCl with water ice. Full symbols correspond to $P_1(t)$ (left-hand ordinate), open symbols correspond to B(t) (right-hand ordinate), and $P_2(t)$ is displayed in the lower panel. The figure displays the result of three simulations of HCl on ice (pulsed-valve experiment) performed at increasing dose at 210 K. (○,●) 10^{13} molecules, (□,■) 7×10^{15} molecules, and (△,▲) 1.5×10^{16} molecules. The input number of reactive sites S_0 is 1.5×10^{15}, corresponding to a surface density of 10^{14} sites cm^{-2}.

duration of approximately 0.5 s, result of the balance between adsorption, desorption and reaction of HCl to B and has practically reached its saturation limit of S_0 (Figure 4, middle part, full squares). At the largest dose of 1.5×10^{16} molecules, the reservoir of bulk species B increases (Figure 4, middle part, open triangles) thus effectively prolonging the saturation of the substrate surface by P_1 and therefore the duration of the steady-state level F_{ss} of the MS signal (Figure 4, upper part). Note that $P_2(t)$ scales with M(t) and that its value is negligible compared to the main bulk species B(t).

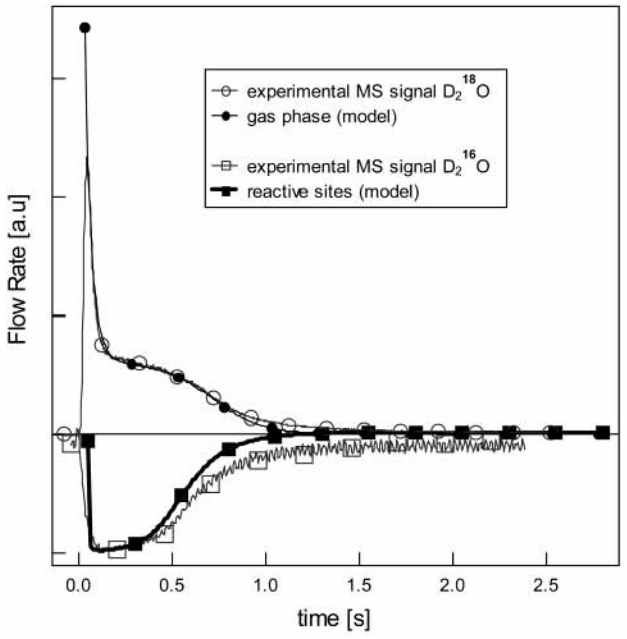

Figure 5. Comparison between an experimental and modeled pulsed-valve experiment of $D_2{}^{18}O$ on $D_2{}^{16}O$ ice at 210 K. The signal corresponding to (□) $D_2{}^{16}O$ comes from the effusing beam of water molecules that evaporate from the ice surface. The MS signal corresponding to gas-phase $D_2{}^{18}O$ is anticorrelated with the (■) modeled number of reactive sites, which means that the surface is practically covered by adsorbed $D_2{}^{18}O$ during the pulse.

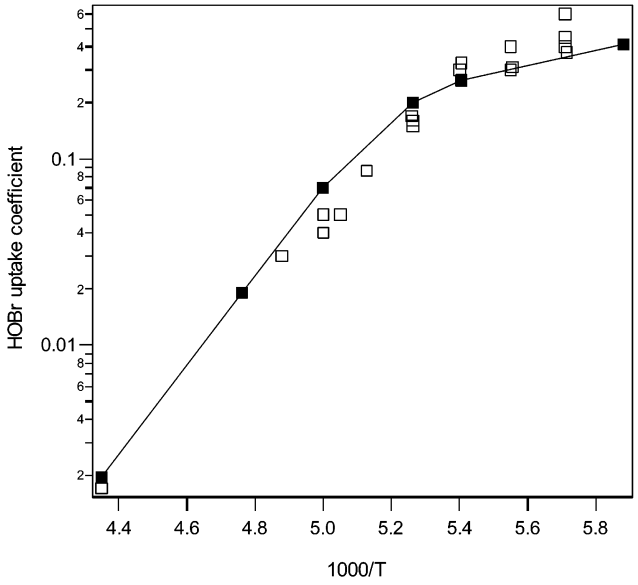

Figure 6. Comparison between (□) experimental and (■) modeled values of the initial uptake coefficient γ_0 of HOBr on bulk ice as a function of temperature. Experimental data are taken from the work of Chaix et al.[28] and Abbatt[25] (value at 228 K). The modeled γ_0 values are obtained using the constants displayed in Table 2 for HOBr (steady-state experiments).

The saturation of the ice substrate has been demonstrated in experiments by Chaix et al.[16] using pulses of labeled $D_2{}^{18}O$ interacting with $D_2{}^{16}O$ ice. Figure 5 displays experimental MS signals for both gas-phase $D_2{}^{18}O$ vapor monitored at *m*/*e* 22 injected in order to probe the $D_2{}^{16}O$ ice matrix whose vapor is monitored at *m*/*e* 20. The condensation of $D_2{}^{18}O$ effectively leads to complete coverage of the $D_2{}^{16}O$ ice matrix during the labeled water pulse as the $D_2{}^{16}O$ evaporation rate comes to a virtual standstill until most of the initially adsorbed $D_2{}^{18}O$ vapor has evaporated. Experimentally, no loss of $D_2{}^{18}O$ by diffusion into the ice matrix is observed at 210 K during the time that $D_2{}^{18}O$ is adsorbed on the ice matrix, because the mass balance between the applied dose of $D_2{}^{18}O$ and the recovered quantity of $D_2{}^{18}O$ corresponding to the integral under the MS signal at *m*/*e* 22 is satisfied. This is in agreement with a low value of the diffusion coefficient for the self-diffusion of H_2O in ice measured under similar experimental conditions.[32] In addition, the MS signal for $D_2{}^{16}O$ closely follows the simulated number of free reactive sites S(*t*) and allows us to relate the steady-state level of gas-phase $D_2{}^{18}O$ to its constant rate of evaporation F_{ev} at a sufficiently large dose of $D_2{}^{18}O$. The equilibrium vapor pressure P_{eq} of M, with M = HCl, HOBr, or $D_2{}^{18}O$, resulting from the equilibrium between adsorption and desorption, does not depend on the dose but only on the temperature of the ice substrate. In this case the absolute value of P_{eq} at $T = 300$ K may be calculated directly from the elementary rate constants in the model as explained in the Appendix and is given by eq 5:

$$P_{eq}(T) = \frac{F_{ev}}{k_{ads}V}RT = \left(\frac{k_{-1}S_o + k_{-3}P_2}{k_3 S_o}\right)\left(\frac{R300}{V}\right) \qquad (5)$$

where P_2 is the saturated value of $P_2(t)$ as displayed in Figure 4, S_0 is the number of reactive sites on the ice substrate, V is the volume of the reactor, and $R = 1.987$ cal/mol. Equation 5 shows that the rate of evaporation depends both on P_1 and P_2 in agreement with Scheme 2, because $P_1 = S_0$ under these conditions. However, the contribution of the term $k_{-3}P_2$ is most often negligible at the used doses or partial pressures used in this work.

A last remark concerns the observation that the rate of uptake on ice is first-order in M under all explored experimental conditions to date despite the complex reaction mechanism displayed in Scheme 2. This comes from the fact that, despite the effective second-order Langmuir adsorption mechanism, the total number of adsorption sites $S_0 = S(t) + P_1(t)$ remains constant throughout the uptake because adsorption takes place both on free sites S(*t*) as well as on occupied sites $P_1(t)$ following sequences I and II, respectively.

Comparison of the Measured Uptake Coefficient and the Vapor Pressure with Model Results. Figures 6−9 compare the measured uptake coefficient with the simulation for HOBr, HCl, HBr, and $D_2{}^{18}O$ interacting with ice as a function of the reciprocal temperature. For the four examples which are all characterized by a negative activation energy to a varying degree, the agreement between experiment and simulation is quite satisfactory. This agreement underlines the need for all the fitting parameters of Scheme 2 because of the large variability of the temperature dependent kinetics as well as the wide range of the measured partial pressures extending over 3 orders of magnitude. The effect of the ice microstructure on the kinetic parameters may be seen in that C-type ice obviously does not support a $D_2{}^{18}O$ vapor pressure in the aftermath of a small $D_2{}^{18}O$ pulse, whereas B-type ice substrates let $D_2{}^{18}O$ molecules evaporate back into the vapor phase. Chaix et al. [16] concluded that the desorption rate of $D_2{}^{18}O$ on $D_2{}^{16}O$ C-type ice was at least 2 orders of magnitude smaller than that obtained on $D_2{}^{16}O$ B-type ice on the basis of transient supersaturation (pulsed-valve) experiments, whereas the difference amounted to a factor of 5 when the condensation/evaporation kinetics was measured using a steady-state approach. Therefore, a large fraction of the condensed $D_2{}^{18}O$ molecules are retained inside the sample of $D_2{}^{16}O$ C-type ice,[38,39] unable to desorb on our

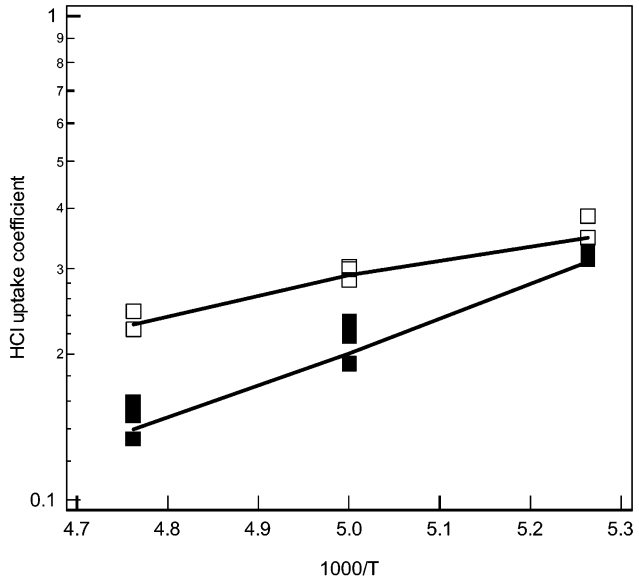

Figure 7. Comparison between (□,■) experimental and (—) modeled values of the initial uptake coefficient γ_0 of HCl on bulk ice (B) as a function of temperature obtained in pulsed-valve experiments. Experimental data are taken from previous work.[20] (□) The values for a low HCl dose ($<10^{15}$ molecules per pulse). (■) The values for a high HCl dose ($>10^{15}$ molecules per pulse). The modeled values are obtained using the constants displayed in Table 2 for HCl (pulsed-valve experiments).

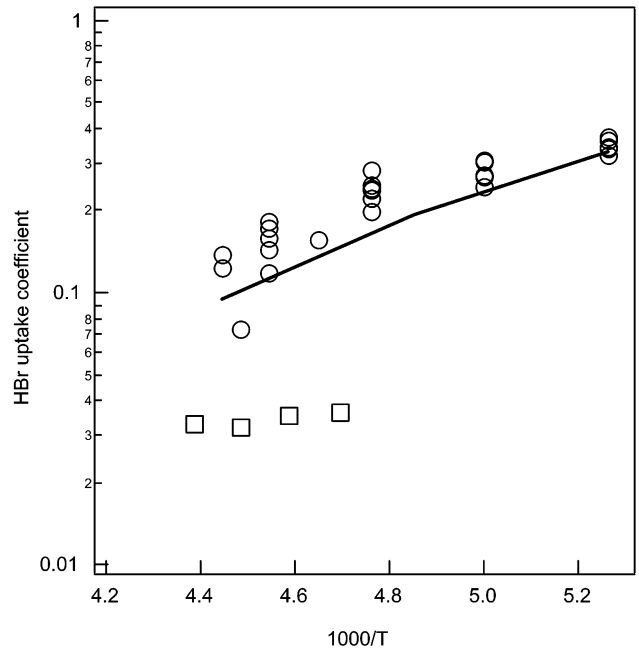

Figure 8. Comparison between the experimental (○,□) and modeled values (solid lines) of the initial uptake coefficient γ_0 of HBr on bulk (B) ice as a function of temperature obtained in both pulsed-valve and steady-state experiments. (○) The values obtained in the Knudsen flow reactor[49] and (□) those obtained by Percival et al.[24] using a coated-wall flow tube. The modeled value is obtained using the constants displayed in Table 2 for HBr (steady-state experiments).

time scale of several seconds in view of the large internal surface of C-type ice, which takes time to be sampled by the finite number of available probe molecules. This goes to show that different growth conditions of ice significantly affect its condensation/evaporation kinetics because structurally different substrates of ice are generated under different growth conditions. A case in point may be the known fact that very low growth

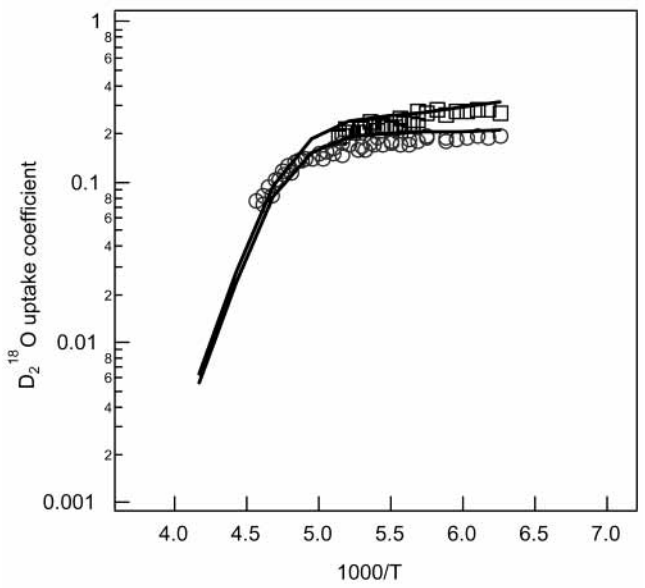

Figure 9. Comparison between the (○,□) experimental and (—) modeled values of the uptake coefficient γ of $D_2{}^{18}O$ on $D_2{}^{16}O$ ice as a function of temperature obtained in pulsed-valve experiments. Experimental data are taken from ref 16. (□) The values obtained on B-type ice and (○) those obtained on vapor-deposited C-type ice. The modeled values represented by the solid lines are obtained using the constants displayed in Table 2 for $D_2{}^{18}O$ (pulsed-valve experiments).

rates lead to metastable amorphous ice structures (I_a) whereas stable hexagonal polycrystalline ices (I_c) are formed at higher growth rates at growth temperatures lower than 77 K.[51,52] This is at variance with results obtained for the growth of most other materials.

This change has been taken into account in the model (see Table 2) by decreasing by 2 orders of magnitude both k_2 and k_{-2} for C-type compared to B-type ice as discussed above, thereby lengthening the time scale for the establishment of equilibrium by a factor of 100 for C-type compared to B-type ice. This increase in time scale is commensurate with the highly structured nature of C-type ice and has to be compared with the experimental time scale of a few seconds for pulsed-valve experiments. This change in time scale may also have to do with the fact that the interface of C-type ice is more disordered compared to B-type ice and that the rearrangement of the P_1 state to B in the k_2 process is therefore slower, hence less probable for C-type than that for B-type ice.

However, this kinetic effect of the lack of an established vapor pressure is certainly not due to an equilibrium isotope effect between ordinary $D_2{}^{16}O$ and labeled $D_2{}^{18}O$. Heras et al.[40] have measured the vapor pressure of $D_2{}^{18}O$-ice at temperatures below 273 K and found it to be slightly lower than the vapor pressure measured above $H_2{}^{16}O$-ice. This change amounts to only a few percent of the vapor pressure[40] and may therefore not account for the kinetic effect observed on C-type ice.

The equilibrium vapor pressure of $D_2{}^{18}O$ over ice is displayed in Figure 10, whose values were calculated according to eq 5 using the fitted kinetic constants displayed in Table 2 resulting from the simulation of pulsed-valve experiments. It leads to values that are in excellent agreement with literature values[41,42] and with experimental values obtained using eqs 1 and 2. The equilibrium vapor pressure therefore represents an important constraint for the kinetic parameters of the model.

In a number of recent laboratory studies the Arrhenius parameters for H_2O evaporation/desorption from ice have been studied over an extended range of temperatures using the

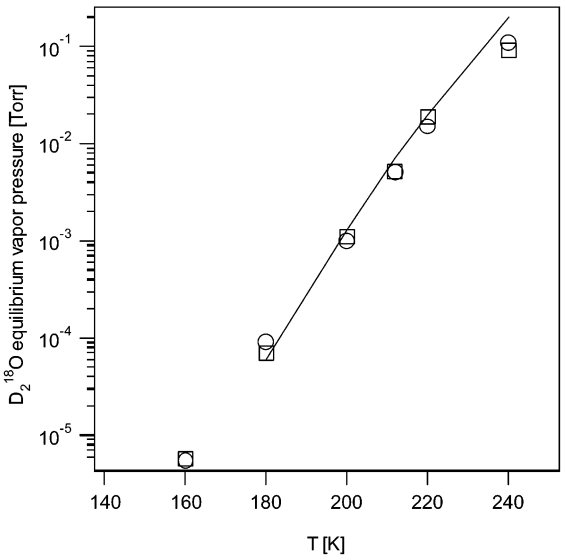

Figure 10. Calculated equilibrium vapor pressure of $D_2{}^{18}O$ on $D_2{}^{16}O$ ice in the temperature range 160−240 K and comparison with (—) the equilibrium vapor pressure according to Jancso et al.[41] (□) The values resulting from the simulation on bulk (B) ice and (○) those resulting from the simulation on condensed (C) ice. The equilibrium vapor pressure is calculated according to eq 5.

classical technique of temperature-programmed desorption (TPD) used for many years in surface science studies.[43,44] The activation energy for desorption E_{des} had been set equal to the enthalpy of reaction given in Scheme 1 whose absolute value corresponds to the enthalpy of sublimation ΔH^0_{subl}.[44] The underlying assumption is that the reverse process of H_2O adsorption according to Scheme 1 has a vanishing activation energy which may however only be true at very low temperatures. In view of our results on the negative activation energy for the condensation of water vapor on ice as displayed in Figure 9, the above assumption is clearly not justified and leads to erroneous values of ΔH^0_{subl}, at least in the atmospherically relevant temperature range 180−273 K. In our opinion thermochemical closure of all processes involved in equilibrium is invaluable in assessing accurate and reliable values of the thermochemical parameters involved. Our approach of separating adsorption/condensation from evaporation/desorption processes is certainly consistent with this requirement.

Figure 11 displays the equilibrium vapor pressure P_{eq}(HCl) of HCl in the reactor as a function of the initial HCl partial pressure $P_{in}(HCl) = F_i(HCl)/(k_{esc}V)RT$. P_{eq}(HCl) is calculated both from experiments and the model according to eq 5. The dependence of P_{eq}(HCl) as a function of P_{in}(HCl) presented in Figure 11 is equivalent to results obtained in pulsed-valve experiments displayed in Figure 4 as far as saturation of the surface and the corresponding rate of desorption is concerned. When P_{eq}(HCl) becomes independent of P_{in}(HCl), the modeled ice surface totally consists of precursors HCl(P_1); hence, $P_1 = S_0$. At this point the HCl in the condensed phase is in equilibrium with its own vapor and P_{eq}(HCl) is numerically equal to the one given by the liquid/ice coexistence curve in the HCl/ice-phase diagram.[34,50] Sequence II in Scheme 2 is therefore the dominant channel of the interaction of HCl with ice from the point on where the ice surface is saturated with HCl(P_1) and corresponds to the equilibrium between condensation and evaporation over a liquid surface or solution.[20] Every additional HCl molecule accommodated on the surface is rapidly transferred into the bulk thereby dissolving additional ice in order to preserve the appropriate concentration of the solution which

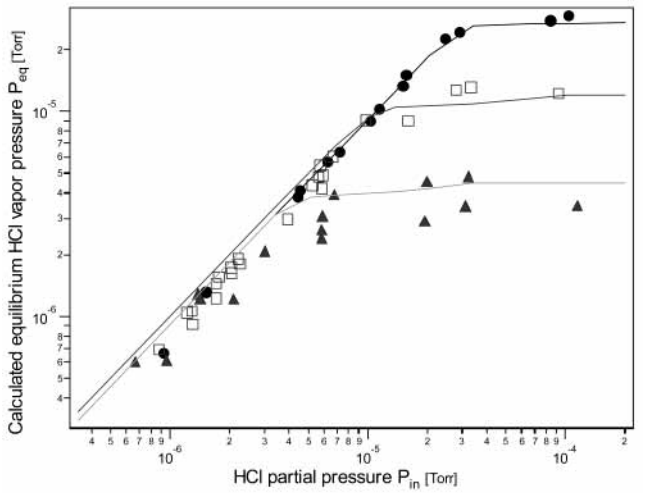

Figure 11. Plot of the calculated HCl equilibrium vapor pressure P_{eq}(HCl) at (▲) 190, (□) 200, and (●) 210 K as a function of the initial partial HCl pressure P_{in}(HCl) in the reactor. Symbols represent experimental data,[20] whereas lines are the calculated values resulting from the model.

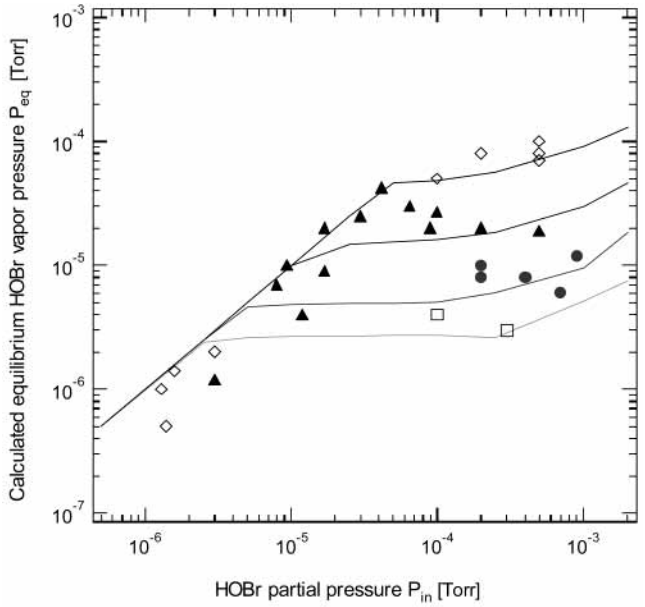

Figure 12. Plot of the calculated HOBr equilibrium vapor pressure P_{eq}(HOBr) at (□) 185, (●) 190 (full circles), (▲) 200, and (◇) 210 K as a function of the initial partial pressure P_{in}(HOBr) in the reactor.[28] Lines are the calculated values resulting from the model.

is only a function of temperature. A van't Hoff plot of P_{eq}(HCl) leads to a reaction enthalpy of $\Delta H^o_r = -8.5 \pm 1.0$ kcal/mol which may be compared to ΔH^o_r calculated from the activation energies of the individual elementary reactions given in Table 2 according to $\Delta H^o_r = E_1 - E_{-1} + E_2 - E_{-2} = -E_{-3}$ resulting in $\Delta H^o_r = -8.4$ kcal/mol. In view of the number of fitted parameters, including their temperature dependence, the agreement is thought to be remarkable.

Figure 12 shows the equilibrium vapor pressure P_{eq}(HOBr) of HOBr as a function of the initial HOBr partial pressure P_{in}(HOBr). The trend of P_{eq}(HOBr) as a function of the partial pressure P_{in}(HOBr) is qualitatively the same as that observed for HCl. We would like to point out, however, that the experiments performed in the Knudsen flow reactor enable the measurement of a vapor pressure in contrast to flow-tube measurements which apparently miss this important feature altogether.[25,27] A van't Hoff plot of P_{eq}(HOBr) leads to a reaction

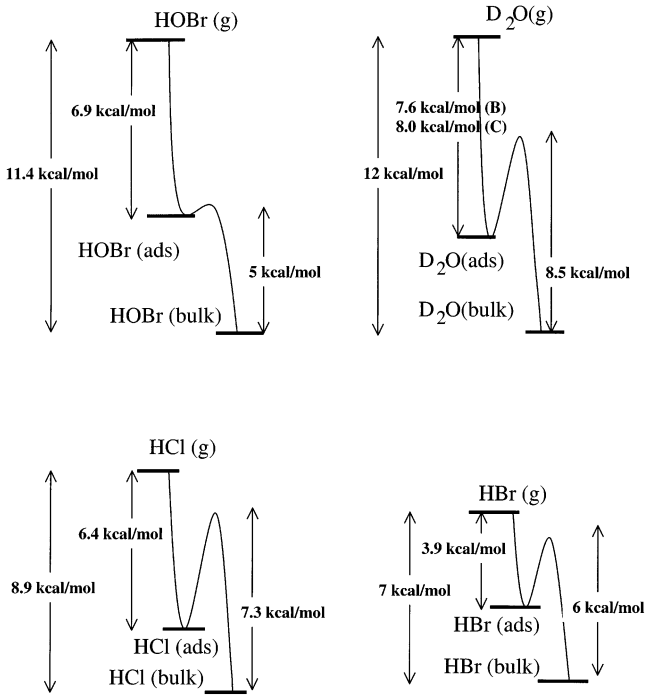

Figure 13. Reaction enthalpy and activation energy for the adsorption of M [M = HOBr(g), D_2O(g), HCl(g), and HBr(g)] on ice according to the mechanism presented in Scheme 2. The reaction enthalpy diagram is constructed from the activation energies determined in simulations (Table 2). The precursor species corresponds to the adsorbed species M_{ads} labeled P_1 in the model. P_2 is not represented, because $\Delta H_f^0(M(bulk)) = \Delta H_f^0(P_2)$ was set in the model.

enthalpy $\Delta H^o_r = -10.5 \pm 1.0$ kcal/mol. The value of ΔH^o_r calculated according to the activation energies derived from the model given in Table 2 results in $\Delta H^o_r = -11.4$ kcal/mol. The agreement between the measured and modeled reaction enthalpy ΔH^o_r is less satisfactory compared to the HCl case discussed above, mainly because of the lack of experimental data for HOBr (see Figure 12).

Figure 13 presents a synopsis of the activation energies of the different elementary processes 1 and 2 of sequence I, Scheme 2, put together in an enthalpy diagram. The analogous processes 3 and 4 would follow an orthogonal reaction coordinate not shown in Figure 13. For M = H_2O, HCl, and HOBr, the good agreement between the modeled and experimentally determined rate parameters has been discussed above, whereas no vapor pressure could be measured for HBr. Nevertheless, temperature-dependent pulsed-valve and steady-state uptake data result in the enthalpy diagram displayed in Figure 13. The central feature of the diagram is a loosely bound precursor whose binding energy $E_{-1} - E_1$ is a significant portion of the overall reaction enthalpy as described in Scheme 1. In all four cases it exceeds 50% of the binding energy of the bulk state and indicates the participation of hydrogen (H)-bonding.[45,46] For instance, H_2O in bulk ice has four hydrogen bonds whereas the precursor P_1 is bound by 7.6 and 8.0 kcal/mol in B- and C-type ice, respectively. This seems to indicate that P_1 is held by less than four hydrogen bonds. For the other members of the series that are bound by two H-bonds analogous conclusions may be drawn. In addition, the barrier E_2 that the precursor state has to overcome in order to rearrange into the bulk (B) state is significant with the exception of the E_2 for HOBr. This latter case has an experimental negative activation energy for HOBr uptake on ice that is essentially identical to the overall reaction enthalpy $E_1 - E_{-1} + E_2 - E_{-2}$, which corresponds to 11.4 kcal/mol. This is indeed a case with very strong negative temperature dependence of the rate of uptake that is rarely encountered in chemical kinetics. Regarding the thermochemistry of sequence II, the simplifying assumption of $\Delta H^0_f(P_2) = \Delta H^0_f$ (B = M_{bulk}) has been made as P_2 is a dimer species of M strongly resembling the bulk state.

TABLE 3: Mass Accommodation Coefficient as a Function of Temperature[a,b]

T (K)	$D_2{}^{18}O$ (B)	$D_2{}^{18}O$ (C)	HOBr (B)	HCl (B)	HBr (B)
190	0.55	0.44	0.86	0.46	0.48
200	0.43	0.34	0.67	0.36	0.38
215	0.20	0.16	0.32	0.18	0.18

[a] B is bulk ice; C is condensed ice (see text). [b] Mass accommodation coefficient calculated according to $\alpha = (k_1S_0 + k_3P_1(t))/\omega = (k_1/\omega)S_0 + (k_3/\omega)(S_0 - S(t))$, where ω = collision frequency at temperature T (see Table 1). At the used concentrations only the first term is important.

The Mass Accommodation Coefficient α. Analogous to energy accommodation the mass accommodation coefficient α, sometimes called the trapping coefficient, describes the efficiency with which the elementary adsorption process k_1 occurs relative to the frequency of gas−surface collisions ω.[47] By virtue of the fact that most gas uptake processes are complex the mass accommodation coefficient α is experimentally accessible only under special conditions.[48] However, it may be calculated according to $\alpha = (k_1S_0 + k_3P_1)/\omega = (k_1/\omega)S_0 + (k_3/\omega)(S_0 - S(t))$, with ω being the collision frequency at temperature T (see Table 1), once we have separated the mechanism into elementary processes as displayed in Table 2. Table 3 displays the values of α as a function of temperature for the molecules M investigated in the present work. A moderate negative temperature dependence may be noted which however does not follow a straight line according to the Arrhenius representation of the temperature dependence of the rates of chemical reactions. The principal reason is that ω is close to its saturation value of 1.0 already at 190 K for all four molecules investigated. The temperature dependence of α is slightly larger (and negative) than the one for S_0 discussed above because of the temperature dependence of ω in the denominator that makes the overall temperature dependence slightly more negative than the one for S_0 by itself. Table 3 displays values whose absolute magnitude is significantly less than unity in the range of atmospheric temperatures. However, they are surprisingly dependent upon temperature. The mass accommodation coefficient α is expected to be essentially independent of temperature on theoretical grounds. However, it is possible that the relative simplicity of Scheme 2 leads to temperature dependent values because of the effect of an as yet unidentified, albeit important, parameter that has not been explicitly included in Scheme 2 and that remains to be discovered in the future.

The BET Adsorption Isotherm for HCl. The dependence of the HCl equilibrium vapor pressure P_{eq}(HCl) as a function of the initial HCl partial pressure $P_{in}(HCl) = F_i(HCl)/(k_{esc}V)$-$RT$ displayed in Figure 11 may be understood in terms of a partial saturation process of the ice substrate. Such a description may be cast in terms of an adsorption isotherm for HCl on ice as displayed in Figure 14. We have used the absolute number of HCl molecules lost to the ice substrate in steady-state experiments at 190 K. The experimental values were determined by numerical integration of the HCl rate of loss $F_r = F_i - F_0$-(t), where $F_0(t)$ is the measured time dependent absolute rate of effusion during the reaction. The integration range from the start of the reaction to the time delay needed to reach the steady-state net rate of uptake typically was a few seconds as displayed in Figure 2 but depended significantly on the flow rate F_i(HCl).

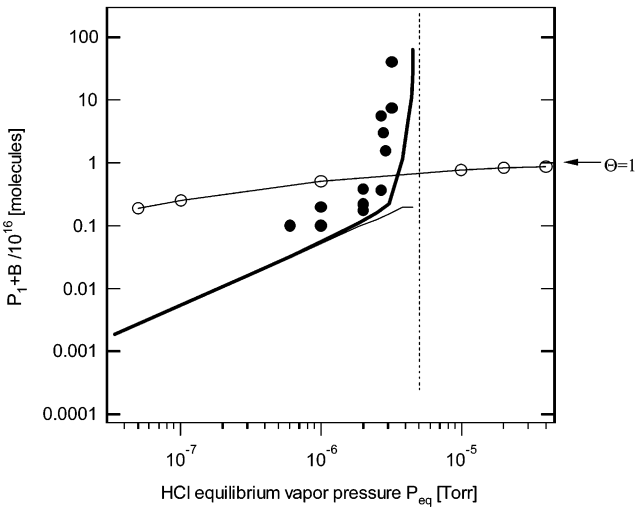

Figure 14. Experimental and modeled adsorption isotherm of HCl on (●) bulk (B) ice at 190. The experimental value corresponds to the number of HCl molecules lost in steady-state experiments during the time needed to reach a steady-state rate of HCl uptake, typically tens of seconds (see Figure 2). The (—) simulated value is the sum of the number of precursor HCl(P_1) and HCl (bulk, B) in the condensed phase for the same time duration. The normal line represents the number of precursors HCl(P_1) tending toward S_0 at high coverages. The vertical dotted line shows the asymptotic value of the number of molecules lost at the corresponding equilibrium vapor pressure. For the sake of comparison, we represented the values obtained from Hynes et al.[21] at (—○—) 190 K.

The value calculated from the model was determined in the same way. We checked the overall mass balance in that the number of molecules lost from the gas phase matched the corresponding amount $P_1 + P_2 + B$ in the condensed phase displayed on the lefthand ordinate of Figure 14 as a check of the numerical calculations. In practice, P_2 is negligible compared to P_1 and B and may therefore be neglected. The modeled quantities of adsorbed HCl agree satisfactorily with the kinetic measurements for $T = 190$ K that have been performed on the basis of both steady-state and pulsed-valve experiments.

Hynes et al.[21] have interpreted their kinetic data of HCl on frozen ice obtained in uptake experiments performed in a coated-wall flow tube using a simple Langmuir isotherm. Figure 14 shows the isotherm at 190 K in comparison with the one obtained using the precursor mechanism presented in Scheme 2. While satisfactory around 10^{-6} Torr of HCl, the simple Langmuir isotherm of Hynes et al. significantly overpredicts adsorbed quantities at lower pressures and underpredicts at pressures in excess of 5×10^{-6} Torr which corresponds to the equilibrium vapor pressure of HCl over ice at 190 K (see Figure 11). It is very clear that a simple isotherm such as used by Hynes et al. is unable to provide a smooth transition between submonolayer and multilayer HCl adsorption such as embodied in Scheme 2 as such a simple approach winds up in gross quantitative and qualitative disagreement with experimental data.

Conclusion

We have presented a master chemical kinetic model that describes the reversible uptake behavior of several molecules in the presence of ice under atmospherically relevant conditions of temperature and for some cases, of concentration. All four molecular systems have common features outlined above and are therefore treated using a common complex chemical mechanism involving two precursors depending on the concentration regime. However, there are interesting differences when considering the branching ratio $r_1 = k_2/k_{-1}$ of sequence I and/or $r_2 = k_4/k_{-3}$ of sequence II of Scheme 2 which are displayed in Table 4. For HBr/ice, r_1 indicates the predominance of reaction, that is, process 2, compared to desorption, which is in agreement with the lack of a vapor pressure in the temperature range studied here and may perhaps be in relation to the propensity of HBr to form crystalline hydrates.[37] For the D_2O/ice interaction, desorption starting from P_1 is predominant and apparently leads to facile evaporation with concomitant establishment of an equilibrium vapor pressure over ice. Owing to the decrease of the rate constant k_2 of C-type ice compared to B-type ice in process 2 discussed above, the propensity of C-type ice to evaporation would seem to be enhanced over that for B-type ice. However, this conclusion is a fallacy because process k_{-2} for C-type ice is also slower by approximately the same amount so that the rate-limiting step in the evaporation of D_2O is k_{-2}. Finally, desorption and reaction are competitive processes for HOBr and HCl interacting with ice.

TABLE 4: Calculated Branching Ratios $r_1 = k_2/k_{-1}$ and $r_2 = k_4/k_{-3}$ (r_2 in Italics) as a Function of Temperature

T (K)	$D_2{}^{18}O$ (B)	$D_2{}^{18}O$ (C)	HOBr (B)	HCl (B)	HBr (B)
190	3.6×10^{-3}	6.5×10^{-5}	4.0	0.68	1.3×10^5
	15.3	*16.1*	*1.1*	*87.8*	*107.4*
200	2.3×10^{-3}	3.9×10^{-5}	1.7	0.56	1.1×10^5
	3.3	*3.44*	*0.24*	*26.3*	*45.3*
215	1.2×10^{-3}	1.8×10^{-5}	0.53	0.43	9.6×10^4
	0.43	*0.45*	*0.031*	*5.64*	*14.5*

Acknowledgment. Generous support of this research was granted by the Fonds National Suisse de la Recherche Scientifique under contract FNS 20-65299.01 and by the Office Fédéral de l'Enseignement et de la Science (OFES) under the EU project CUTICE.

Appendix

The rate of change of the gas-phase concentration M(t) (unit of total number of molecules) is given for steady-state experiments according to

$$dM(t)/dt = -k_{esc}M(t) - k_1M(t)(S_0 - P_1(t)) + k_{-1}P_1(t) - k_3M(t)P_1(t) + k_{-3}P_2(t) + F_i \quad (6)$$

At steady-state conditions ($dM(t)/dt = 0$) we may express the net measured rate of uptake F_{ss} in terms of eq 7, assuming that all or nearly all reactive sites are occupied by P_1 such that it effectively becomes constant; thus, $P_1 = S_0$:

$$F_{ss} = M_{ss}k_{esc} = \left(\frac{k_{esc}}{k_{esc} + k_3P_1}F_i\right) + \left(\frac{k_{-1}P_1 + k_{-3}P_2}{k_{esc} + k_3P_1}\right)k_{esc} \quad (7)$$

We compare F_{ss} from eq 3 with F_{ss} from eq 7 and arrive at eq 8:

$$F_{ss} = \left(\frac{k_{esc}}{k_{esc} + k_{ads}}F_i\right) + \left(\frac{k_{esc}}{k_{esc} + k_{ads}}F_{ev}\right) \quad (8)$$

Under these conditions, $k_{ads} = k_3P_1$ because process 1 is saturated, and $F_{ev} = k_{-1}P_1 + k_3P_2$, which is related to F_{ss} obtained in the pulsed-valve experiments where $F_i = 0$ in eq 3.

The comparison of eq 7 with eq 8 obtains the relationship between F_{ev} and the kinetic parameters used in the kinetic master equation given in eq E-1 and leads to the following expression for the (calculated) equilibrium vapor pressure of M over ice

under the assumption of complete saturation of the ice substrate, that is, $P_1 = S_0$:

$$F_{ev} = k_{-1}P_1 + k_{-3}P_2; \quad P_{eq} = \frac{k_{-1}P_1 + k_{-3}P_2}{k_3P_1}\left(\frac{RT}{V}\right) \quad (9)$$

References and Notes

(1) Solomon, S.; Garcia R. R.; Rowland F. S.; Wuebbles D. J. *Nature* **1986**, *321*, 755.

(2) Turco R.; Toon, O. B.; Hamill P. *J. Geophys. Res.* **1989**, *94*, 16493.

(3) Jensen E. J.; Read W. G.; Mergenthaler J.; Sandor B. J.; Pfister, L.; Tabazadeh A. *Geophys. Res. Lett.* **1999**, *26*, 2347.

(4) Mergenthaler, J. L.; Roche A. E.; Kumer J. B. *J. Geophys. Res.* **1999**, *194*, 22183.

(5) Schumann U.; Ström J.; Busen R.; Baumann R.; Gierens K.; et al. *J. Geophys. Res.* **1996**, *101*, 6853.

(6) Minnis, P.; Schumann U.; Doelling D. R.; Gierens K. M.; Fahey D. W. *Geophys. Res. Lett.* **1999**, *26*, 1853.

(7) Sausen, R.; Gierens K.; Ponater M.; Schumann U. *Theor. Appl. Climatol.* **1998**, *61*, 127.

(8) Penner, J. E., Lister D. H., Griggs D. J., Dokken D. J., McFarland M., Ed. *Aviation and the Global Atmosphere*; Cambridge University Press: Cambridge, U.K., 1999.

(9) Shindell, D. T.; Rind D.; Lonergan P. *Nature* **1998**, *392*, 589.

(10) Johnson, C. E.; Stevenson, D. S.; Collins W. J.; Derwent R. G. *Geophys. Res. Lett.* **2001**, *28*, 1723.

(11) Zondlo, M. A.; Hudson P. K.; Prenni A. J.; Tolbert, M. A. *Annu. Rev. Phys. Chem.* **2000**, *51*, 473.

(12) Solomon S.; Borrmann S.; Garcia R. R.; Portmann R.; Thomason L.; Poole, L. R.; Winker D.; McCormick M. P. *J. Geophys. Res.* **1997**, *102*, 21411.

(13) Leu, M.-T. *Geophys. Res. Lett.* **1988**, *15*, 17.

(14) Haynes, D. R.; Tro, N. J.; George S. M. *J. Phys. Chem.* **1992**, *96*, 8504.

(15) Brown, D. E.; George, S. M.; Huang, C.; Wong, E. K. L.; Rider, K. B.; Scott Smith, R.; Kay, B. D. *J. Phys. Chem.* **1996**, *100*, 4988.

(16) Chaix, L.; van den Bergh, H.; Rossi, M. J. *J. Phys. Chem. A* **1998**, *102*, 10300.

(17) Leu, M.-T.; Moore, S. B.; Keyser, L. F. *J. Phys. Chem.* **1991**, *95*, 7763.

(18) Hanson, D. R.; Ravishankara, A. R. *J. Phys. Chem.* **1992**, *96*, 2682.

(19) Chu, L. T.; Leu, M.-T.; Keyser, L. F. *J. Phys. Chem.* **1993**, *97*, 7779.

(20) Fluckiger, B.; Thielmann, A.; Gutzwiller, L.; Rossi, M. J. *Ber. Bunsen-Ges. Phys. Chem.* **1998**, *102*, 915.

(21) Hynes, R. G.; Mössinger, J. C.; Cox, R. A. *Geophys. Res. Lett.* **2001**, *28*, 2827.

(22) Hanson, D. R.; Ravishankara, A. R. *J. Phys. Chem.* **1992**, *69*, 9441.

(23) Seisel; S.; Rossi, M. J. *Ber. Bunsen-Ges. Phys. Chem.* **1997**, *101*, 943.

(24) Percival, C. J.; Mössinger, J. C.; Cox, R. A. *Phys. Chem. Chem. Phys.* **1999**, *1*, 4565.

(25) Abbatt, J. P. D. *Geophys. Res. Lett.* **1994**, *21*, 665.

(26) Allanic, A.; Oppliger, R.; Rossi, M. J. *J. Geophys. Res.* **1997**, *102*, 23529.

(27) Chu, L.; Chu, L. T. *J. Phys. Chem. A* **1999**, *103*, 8640.

(28) Chaix, L.; Allanic, A.; Rossi, M. J. *J. Phys. Chem. A* **2000**, *104*, 7268.

(29) Golden, D. M.; Spokes, G. N.; Benson, S. W. *Angew. Chem., Int Ed.* **1973**, *12*, 534.

(30) Caloz, F.; Fenter F. F.; Tabor K. D.; Rossi, M. J. *Rev. Sci. Instrum.* **1997**, *8*, 3172; *Rev. Sci. Instrum.* **1997**, *8*, 3180.

(31) The terminology used throughout this paper is the following: If M interacts with its own condensed phase, such as $M = H_2O$, with pure water ice, the heterogeneous reactions with respect to the gas-phase concentration of M are called condensation and evaporation. For every other case, the reactions are called adsorption and desorption, respectively.

(32) Fluckiger, B.; Chaix, L.; Rossi, M. J. *J. Phys. Chem. A* **2000**, *104*, 11739.

(33) Berland, B. S.; Tolbert M. A.; George S. M. *J. Phys. Chem. A* **1997**, *101*, 9954.

(34) Abbatt, J. P. D.; Beyer, K. D.; Fucaloro, A. F.; McMahon, J. R.; Wooldridge, P. J.; Zhang, R.; Molina, M. J. *J. Geophys. Res.* **1992**, *97*, 15819.

(35) Braker, W.; Mossman, A. L. *Matheson Gas Data Book*, sixth ed. 1980, Matheson Inc.

(36) Lee, S.-H.; Leard D. C.; Zhang R.; Molina L. T.; Molina, M. J. *Chem. Phys. Lett.* **1999**, *315*, 7.

(37) Chu, L. T.; Heron, J. W. *Geophys. Res. Lett.* **1995**, *22*, 3211.

(38) Keyser, L. F.; Leu, M. T. *J. Colloid Interface Sci.* **1993**, *155*, 137.

(39) Keyser, L. F.; Leu, M. T. *J. Phys. Chem. B* **1997**, *101*.

(40) Heras, J. M.; et al. *Chem. Scr.* **1983**, *23*, 244.

(41) Jancso, G.; Pupezin, J.; Van Hook, W. A. *J. Chem. Phys.* **1970**, *710*, 2984.

(42) Marti, J.; Mauersberger, K. *Geophys. Res. Lett.* **1993**, *20*, 359.

(43) Koehler, B. G. *Int. J. Chem. Kinet.* **2001**, *34*, 295.

(44) Fraser, H.; Collings, M. P.; McCoustra, M. R. S.; Williams, D. A. *Mon. Not. R. Astron. Soc.* **2001**, *327*, 1165.

(45) Devlin, J. P.; Uras, N.; Sadlej J.; Buch V. *Nature* **2002**, *417*, 269.

(46) Uras-Aytemiz N.; Joyce C.; Devlin J. P. *J. Phys. Chem. A* **2001**, *105*, 10497.

(47) Morris, J. R.; Behr, P.; Antman, M. D.; Ringeisen, B. R.; Splan, J.; Nathanson G. M. *J. Phys. Chem. A* **2000**, *104*, 6738.

(48) Worsnop, D.; Zahniser, M. S.; Kolb, C. E.; Gardner, J. A.; Watson, L. R.; Van Doren, J. M.; Jayne, J. T.; Davidovits, P. *J. Phys. Chem.* **1989**, *93*, 1159.

(49) Fluckiger, B. Ph.D. Thesis 2158, Ecole Polytechnique Fédérale de Lausanne, Lausanne, 2000.

(50) Molina, M. J. The Probable Role of Stratospheric "Ice" clouds: Heterogeneous Chemistry of the "Ozone Hole". In the *Chemistry of the Atmosphere: its Impact on Global Change*; Calvert, J. G., Ed.; Blackwell Scientific: Boston, MA, 1994; p 27.

(51) Olander, D. S.; Rice, S. A. *Proc. Natl. Acad. Sci. U.S.A.* **1972**, *69*, 98.

(52) Sivakumar, T. C.; Rice, A. A.; Sceats, M. C. *J. Chem. Phys.* **1978**, *69*, 3468.